Experimental estimation of stored stress within spherical microtissues

Thierry Colin, Guillaume Dechristé, Jérôme Fehrenbach, Ludivine Guillaume, Valérie Lobjois, Clair Poignard

JMB manuscript No.
(will be inserted by the editor)

Experimental estimation of stored stress within spherical microtissues

What can and cannot be inferred from cutting experiments

Thierry Colin · Guillaume Dechristé · Jérôme Fehrenbach · Ludivine Guillaume · Valérie Lobjois · Clair Poignard

Received: date / Accepted: date

Abstract Biological tissues accumulate mechanical stress during their growth. The mere measurement of the stored stress is not an easy task. We address here the spherical case and our experiments consist in performing an incision of a spherical microtissue (tumor spheroid) grown *in vitro*. On the theoretical part we derive a compatibility condition on the stored stress in spherical symmetry, which imposes a relation between the circumferential and radial stored stress. The numerical implementation uses the hyperelastic model of Ciarlet and Geymonat. A parametric study is performed to assess the influence of each parameter on the shape of the domain after the incision. As a conclusion, the total radial stored stress can be confidently estimated from the measurement of the opening after incision. We validate the approach with experimental data.

Keywords Spherical microtissues · Stored stress · Hyperelasticity · Parametric study

Mathematics Subject Classification (2010) 35Q74 · 74B20 · 74L15

This work was supported by the CNRS, Université Paul Sabatier, ITMO Cancer AVIESAN (Alliance Nationale pour les Sciences de la Vie et de la Santé, National Alliance for Life Sciences & Health) within the framework of the Cancer Plan and la Ligue Contre le Cancer (comité de la Haute-Garonne). The authors wish to acknowledge the TRI-Genotoul and ITAV imaging facilities. We thank Bernard Ducommun for his helpful comments on the manuscript and the members of our groups for discussions and interest to this project.

Th. Colin, G. Dechristé, C. Poignard
Team MONC, INRIA Bordeaux-Sud-Ouest, Institut de Mathématiques de Bordeaux, CNRS UMR 5251 & Université de Bordeaux,
351 cours de la Libération, 33405 Talence Cedex, France
E-mail: {Thierry.Colin,guillaume.dechriste}@math.u-bordeaux1.fr;clair.poignard@inria.fr

J. Fehrenbach, L. Guillaume, V. Lobjois
Université de Toulouse, ITAV, CNRS, UPS, Toulouse, France.
E-mail: jerome.fehrenbach@math.univ-toulouse.fr; {Valerie.LOBJOIS, Ludivine.GUILLAUME}@itav.fr

1 Introduction

Position of the problem and previous work. Physical forces play a crucial role in tissue development and in the control of adult tissue homeostasis [4,16]. A tissue is an organized population of cells that grow and deform to create and maintain a defined 3D shape. The deformation and re-organization of the tissue occurs at a faster time scale than tissue growth, hence at a given time the tissue can be considered in quasi-static equilibrium. This implies the existence of intrinsic mechanical forces and a precisely tuned balance that maintains homeostatic tension. Sensing compression and tension forces (i.e., mechano-sensing) is an important component of cell physiology, hence a change in mechanical homeostasis within tissues is associated with several diseases and has been observed during tumor growth.

In a seminal work on blood vessels Fung and collaborators have shown [5] the fundamental importance of the residual stress in tissues. The residual stress is defined as the remaining stress in a body when all the external loads have been removed. The state considered here is the unloaded state to determine the residual stress, but *in vivo* this zero-stress state is unreachable and no strain gauge exists. Thus, currently there is no method to measure *in vivo* the residual stress. Making incisions in a tissue *ex vivo* and observing any resulting changes of shape can reveal the presence of residual stress. By using this experimental method, Fung *et al.* have shown the presence of residual stress in the cardiovascular system (arteries [5,15], veins [24], ventricular myocardium [19]) and trachea [11]. An important conclusion of these works is that the level of internal stress and strain of organs guide the physiological functions.

As in other tissues, residual stress in solid tumors is not measurable *in vivo*. Jain and collaborators applied the concept presented above and have shown by relaxation experiments after cutting *ex vivo* murine tumors from different cell lines and also on human tumors (sarcoma) that solid tumors are also characterized by an intrinsic growth-induced solid stress [23].

Numerous models have been proposed to account for the interplay between tissue growth and mechanical stress, the reader is referred to the review [14] for detailed material and references. Remodelling occurs during tissue growth and can be accounted for by microscopic models as well as continuous models, *e.g.* by considering multiphasic materials [2,10]. The aim of the present work is not to describe the accumulation of stress as time evolves, but rather to estimate at a given instant the stress in the domain. The reason is that our measurements are obtained by destructive experiments similar to Fung's setup, it is therefore not possible to follow the history of one sample. In this framework it makes sense to use a continuous model and consider the tissue as a hyperelastic solid (composed of one phase). The stored stress is described by a tensor field F^o which is locally the deformation gradient from the reference stress free configuration. The multiplicative decomposition $F^o = F_e F_g$, where F_g is the growth tensor and F_e is the accomodation tensor is known as the Bilby-Gardner-Stroh-Kröner-Lee decomposition [18]. The description at longer time scale to account for growth or remodelling after the incision of the domain

should incorporate more complex models, *e.g.* multiphasic models or poro-elasto-plastic models [1]. This is not in the scope of the present work.

Main contributions. We propose a method to estimate the accumulated stored stress in a spherical tissue domain based on cutting experiments. The available information in an ideal experiment is the shape of the domain after the incision, and the question addressed in the present work is to determine what quantities regarding the stored stress can be inferred from the observation of the shape of the domain. We use the fact that the domain is initially (before the incision) under quasi-static equilibrium to derive compatibility conditions on the stored stress. These compatibility conditions were first proposed in [13] and we adapt them to spherical symmetry. In other words the spatial distribution of stored stress cannot be arbitrary and we precisely describe the admissible distributions of stored stress, by providing a relation that must be satisfied between radial and circumferential stored stresses. To the best of our knowledge this relation is new. We provide also the methodological material necessary to perform simulations of stored stress, using a particular strain energy density proposed by Ciarlet and Geymonat [7]. We perform a parametric study to estimate the influence of each parameter of the model on the simulation results. A parameter that has a tiny influence on the result of the simulation can not be recovered confidently since any value of this parameter in its range predicts similar results. This parametric study allows us to assess which mechanical parameters can be inferred from the experiments.

In our case the experiment consists in the incision of spherical microtissues, with typical scale a few hundreds micrometers. We used multicellular spheroids, *in vitro* models that reproduce the 3D architecture of tissues or tumor micro-domains. They represent versatile avatar that are widely used in pharmacological evaluation or tissue engineering [8]. We observe a large variability in the shape of the domain after incision, mainly due to experimental bias (the cutting plane is not always perfectly a symmetry plane) and sample variability. We thus boil down the measured data to two numeric quantities: opening length vs incision depth. We show that it is then possible to estimate confidently the total radial stored stress. Our approach is validated by a comparison with experimental results.

The present paper is somehow a proof of concept. In a forthcoming work we will apply the methodology presented here to different *in vitro* experiments and derive new biological understanding on mechanical stresses on tumors 3D models.

Organization of the paper. In Section 2 we present the modelling of the stored stress that will be used in the sequel, together with a discussion in the case of spherical symmetry. We describe in Section 3 the hyperelastic model that we will use, following Ciarlet and Geymonat [7]. The parametric study is detailed in Section 4. Finally we demonstrate the ability of our model to provide quantitative estimates of stored stress, by analyzing the results of one experiment in Section 5.

2 Stored stress

2.1 The experimental approach

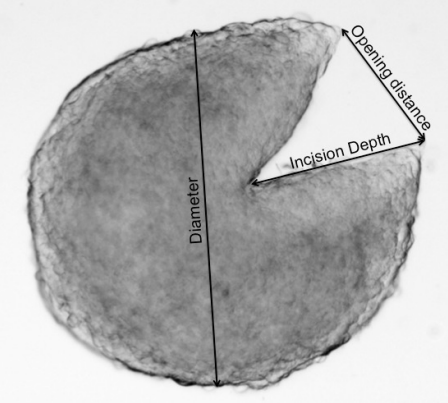

Fig. 1 Incisions depth and opening length. In practice the incision depth is obtained as the average of the lengths of both sides of the incision.

In the present work we estimate and characterize the accumulated stored stress within a spherical microtissue by a quantitative comparison between *in vitro* experiments and *in silico* simulations. *In vitro* experiments were performed on multicellular spheroids made of HCT116 colon carcinoma cells. The spheroid is initially considered at rest, and the medium is pre-stressed. The *in silico* and *in vitro* experiments consist of cutting the spheroid, either in two halves or partially along a half plane. This incision has the effect of partially releasing the stored stress leading to the opening of spheroids. We define in Figure 1 the incision depth and opening length after cutting.

2.2 Notation

We consider the domain at a given instant and we assume that the tissue is a hyperelastic medium at the time scale of our observation. This means that neither active mechanical behaviour, nor viscoelastic effects (that occur at a longer time scale) are considered.

Before the incision, the spherical domain of the tissue is denoted Ω. The domain is at rest under homogeneous Neumann boundary condition, and we neglect the gravity so there is no volume load. Let $\mathbf{u}(\mathbf{x})$ denote the displacement of the point $\mathbf{x} \in \Omega$. The position $\mathbf{x}$ is the reference position of the material point and its position after the displacement is $\mathbf{x} + \mathbf{u}(\mathbf{x})$.

Modelling the tissue as a hyperelastic solid undergoing finite deformations amounts to assume that the configuration under given external loads minimizes

the mechanical energy. This energy is given as the integral over Ω of a local density energy $W = W(F)$ where the deformation gradient F is given by $F = Id + \nabla \mathbf{u}$ and W depends on the mechanical model. The reader is referred to [6,17] for a detailed presentation. This description is valid when the reference configuration corresponds to a stress-free state. We describe in Section 2.3 the case of prestressed material.

If we assume that the medium is isotropic then the local energy density depends only on the principal invariants i_1, i_2, i_3 of the right Cauchy-Green strain tensor $C = F^T F$. The invariants of the right Cauchy-Green tensor are

$$\begin{aligned} i_1(C) &= \mathrm{Tr}(C), \\ i_2(C) &= \mathrm{Tr}(adj(C)) = \frac{1}{2}(\mathrm{Tr}(C)^2 - \mathrm{Tr}(C^2)), \\ i_3(C) &= \det(C). \end{aligned} \tag{1}$$

The precise form of $W(F) = \mathcal{W}(i_1(C), i_2(C), i_3(C))$ that we use in our simulations will be detailed in Section 3.1, and for the moment we provide general considerations.

The minimization of

$$\mathcal{E}(\mathbf{u}) = \int_\Omega \mathcal{W}(i_1(C), i_2(C), i_3(C))\, dx$$

can be achieved by satisfying the following Euler-Lagrange conditions:

$$\begin{cases} \mathrm{div}(FS) = 0 & \Omega, \\ \text{Dirichlet/Neumann boundary cond.} & \partial\Omega, \end{cases}$$

where $S = 2\dfrac{\partial \mathcal{W}}{\partial C}$ is the second Piola Kirchhof stress tensor.

2.3 Constitutive equation for a prestressed hyperelastic isotropic material

Our description of the stored stress accumulated in growing tissues follows the description of residual stresses provided in [13]. In the present section we describe the approach of [13] and its application to hyperelastic materials. At the neighborhood of the point $\mathbf{x}$ in the reference configuration the medium is obtained from a virtual stress free reference configuration by a stored strain F^o, see Figure 2. The tensor field F^o induces a stored stress through the constitutive equation of the medium. Note that, following [13], at each point $\mathbf{x}$ there is a local tensor field $F^o(\mathbf{x})$ that describes the local stored strain. This local deformation gradient is not necessarily the gradient of a global $\mathbf{u}^o$. In the sequel we omit to write explicitly the dependence on $\mathbf{x}$.

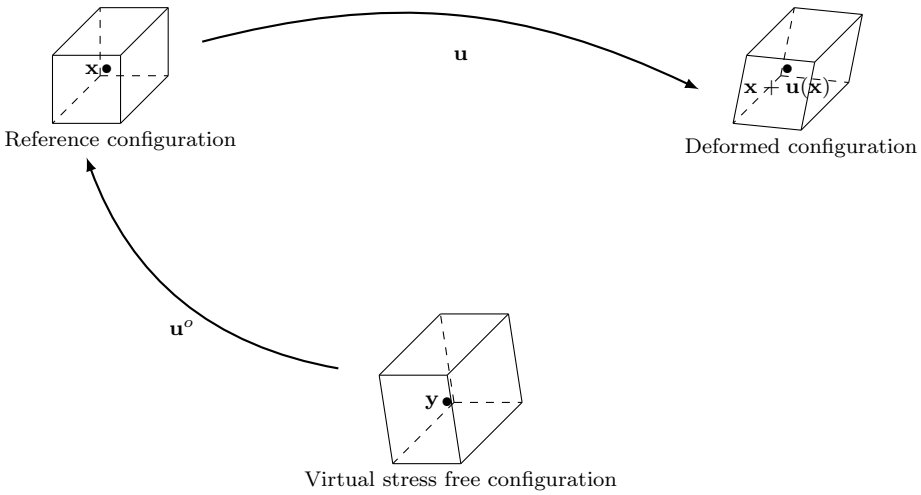

Fig. 2 Representation of an infinitesimal neighborhood of a point $\mathbf{x}$ in the different configurations describing the stored stress, following the presentation in [13]. The reference configuration represents the medium at rest, which means without displacement but possibly with accumulated stress. When released from the stress exerted from the surrounding medium, the infinitesimal neighborhood relaxes to a (virtual) stress free configuration. The accumulated stress is described by the deformation gradient F^o from the virtual stress free configuration to the reference configuration. The neighborhood of $\mathbf{x}$ is distorted through the displacement field $\mathbf{u}$. The constitutive equation for the medium with accumulated stress is obtained from the constitutive hyperelastic law of the medium, and the deformation from the stress free configuration to the deformed configuration is FF^o, where $F = Id + \nabla\mathbf{u}$.

When the deformation from the reference configuration is $\mathbf{u}$, and the local deformation gradient is $F = Id + \nabla\mathbf{u}$ then the deformation gradient from the stress-free configuration is FF^o. Therefore the local energy density is

$$W'(F) = \frac{1}{\det F^o} W(FF^o) = \frac{1}{\det F^o} \mathcal{W}(i_1(C^o), i_2(C^o), i_3(C^o)),$$

where the $i_k(C^o)$ are the invariants of the prestrained right Cauchy-Green strain tensor

$$C^o = (FF^o)^T FF^o = F^{oT} F^T FF^o.$$

The factor $\dfrac{1}{\det F^o}$ accounts for the local change of volume between the virtual stress free configuration and the reference configuration. The displacement field $\mathbf{u} \in H^1(\Omega, \mathbf{R}^3)$ minimizes the total energy

$$\mathcal{E}^o(\mathbf{u}) = \int_\Omega \frac{1}{\det F^o} \mathcal{W}(i_1(C^o), i_2(C^o), i_3(C^o)) dx.$$

The Euler-Lagrange equation that expresses the stationarity of $\mathcal{E}^o$ at $\mathbf{u}$ reads

$$\forall \varphi \in H^1(\Omega, \mathbf{R}^3), \quad D\mathcal{E}^o(\mathbf{u}).\varphi = 0. \tag{2}$$

For all φ we have:

$$D\mathcal{E}^o(\mathbf{u}).\varphi = \int_\Omega \frac{1}{\det F^o}\left(\partial_1\mathcal{W}.Di_1(C^o).\varphi + \partial_2\mathcal{W}.Di_2(C^o).\varphi + \partial_3\mathcal{W}.Di_3(C^o).\varphi\right) dx.$$

The prestrained invariants are provided below together with their derivatives which are obtained using tedious but straightforward calculations:

$$\begin{aligned}
i_1(C^o) &= \mathrm{Tr}(F^{oT}F^TFF^o),\\
Di_1(C^o).\varphi &= 2FF^oF^{oT} : \nabla\varphi,\\
i_2(C^o) &= \frac{1}{2}(\mathrm{Tr}(F^{oT}F^TFF^o)^2 - \mathrm{Tr}((F^{oT}F^TFF^o)^2)),\\
Di_2(C^o).\varphi &= 2F\left[\mathrm{Tr}(C^o)F^oF^{oT} - F^oF^{oT}F^TFF^oF^{oT}\right] : \nabla\varphi,\\
i_3(C^o) &= \det(F^{oT}F^TFF^o),\\
Di_3(C^o).\varphi &= 2\det(F^{oT}F^o)\det(F^TF)FC^{-1} : \nabla\varphi.
\end{aligned}$$

Therefore Equation (2) reads

$$\forall\varphi \in H^1(\Omega,\mathbf{R}^3), \quad \int_\Omega FS^o : \nabla\varphi\, dx = 0.$$

where

$$S^o = \frac{2}{\det F^o}\left(\partial_1\mathcal{W}F^oF^{oT} + \partial_2\mathcal{W}\left[\mathrm{Tr}(C^o)F^oF^{oT} - F^oF^{oT}F^TFF^oF^{oT}\right] + \partial_3\mathcal{W}\det(F^{oT}F^o)\det(F^TF)C^{-1}\right).$$

An integration by parts yields

$$\mathrm{div}(FS^o) = 0 \quad \text{in } \Omega.$$

Note: the experimental boundary condition is homogeneous Neumann (the sample is free to move), but on the mathematical point of view it is desirable to have uniqueness of the solution. Uniqueness is ensured in the space $H^1(\Omega,\mathbf{R}^3)/SE_3$ where SE_3 is the group of positive isometries of the Euclidean 3-space. On the numerical point of view, uniqueness is enforced by defining a fixed point (homogeneous Dirichlet condition) at the center of the sphere, a homogeneous Dirichlet condition in the x direction for the nadir -the point with coordinates (0,0,-1)- and a zero angular momentum w.r.t. two orthogonal axes to prevent translations and rotations. This amounts to restrict admissible displacements to a subspace of $H^1(\Omega,\mathbf{R}^3)$ of co-dimension 6.

2.4 Admissible stored stress under spherical symmetry

Following [13] there is a compatibility condition on the stored stress that comes from the fact that the medium is under elastic equilibrium (before we

start cutting it), in other words $F = Id$ solves the equilibrium equation. This condition reads

$$\begin{cases} \mathrm{div}(T) = 0 & \Omega, \\ T.n = 0 & \partial\Omega, \end{cases} \tag{3}$$

with

$$T = \frac{2}{\det F^o}(\partial_1\mathcal{W} + \partial_2\mathcal{W}\mathrm{Tr}(F^o F^{oT}))F^o F^{oT} - \frac{2}{\det F^o}\partial_2\mathcal{W}F^o F^{oT} F^o F^{oT} + 2\det F^o \partial_3\mathcal{W} Id. \tag{4}$$

In our experiments, the domain is a sphere, which can be assumed to be the unit sphere, up to a change of space unit. We assume that all the quantities of interest possess spherical symmetry, and we use spherical coordinates (r, θ, φ). In particular the right Cauchy-Green tensor at rest reads

$$F^o F^{oT} = Id + \alpha(r) e_r \otimes e_r + \beta(r)(e_\theta \otimes e_\theta + e_\varphi \otimes e_\varphi), \tag{5}$$

where $\alpha(r)$, resp. $\beta(r)$, denote the magnitude of the compressive, resp. circumferential, stored strain. In order to write the equilibrium equation we will use the following quantities:

$$\mathrm{Tr}(F^o F^{oT}) = 3 + \alpha(r) + 2\beta(r),$$

and

$$(\det F^o)^2 = (1 + \alpha(r))(1 + \beta(r))^2.$$

Therefore Equation (4) in spherical coordinates reads, when we denote for simplicity α and β for $\alpha(r)$ and $\beta(r)$:

$$\begin{aligned} T = {} & \frac{2}{\det F^o}(\partial_1\mathcal{W} + \partial_2\mathcal{W}(3 + \alpha + 2\beta)) \begin{pmatrix} 1+\alpha & 0 & 0 \\ 0 & 1+\beta & 0 \\ 0 & 0 & 1+\beta \end{pmatrix} \\ & - \frac{2}{\det F^o}\partial_2\mathcal{W} \begin{pmatrix} (1+\alpha)^2 & 0 & 0 \\ 0 & (1+\beta)^2 & 0 \\ 0 & 0 & (1+\beta)^2 \end{pmatrix} + \frac{2}{\det F^o}\partial_3\mathcal{W}(1+\alpha)(1+\beta)^2 Id \\ = {} & \begin{pmatrix} T_{11} & 0 & 0 \\ 0 & T_{22} & 0 \\ 0 & 0 & T_{22} \end{pmatrix}, \end{aligned}$$

where the coefficients $T_{11} = T_{11}(r)$ and $T_{22} = T_{22}(r)$ depend on the stored strain distribution through α and β, and on the constitutive law of the material. The radial stored strain $\alpha(r)$ and the circumferential stored strain $\beta(r)$ cannot be arbitrary since they are related by the fact that the medium is at rest before the incision: Equation (3) reads in spherical coordinates

$$T_{11}' + \frac{1}{r}(2T_{11} - 2T_{22}) = 0, \tag{6}$$

where T_{11}' denotes the derivative of T_{11}. This approach provides an explicit compatibility condition between radial and circumferential stored stress whatever the constitutive law of the material is. We give the precise form of this compatibility condition in terms of stored strains in the case of Ciarlet-Geymonat material below.

3 The mechanical model

3.1 Ciarlet-Geymonat model

We consider a Ciarlet-Geymonat model [7] which is a realistic model of 3D deformations. It models a hyperelastic material with the following energy density:

$$W(F) = ai_1(C) + \left(\frac{\mu}{2} - a\right) i_2(C) + \left(\frac{\lambda}{4} - \frac{\mu}{2} + a\right) i_3(C) - \left(\frac{\mu}{2} + \frac{\lambda}{4}\right) \ln(i_3(C)), \tag{7}$$

where λ, μ and a describe the material and i_1, i_2, i_3 are the invariants defined in Equation (1). When the strain tends to 0, this is asymptotic to a linear material satisfying Hooke's law with Lamé parameters λ, μ. The constitutive parameters are required to satisfy the following constraints:

$$\lambda, \mu > 0, \qquad \max(0, \frac{\mu}{2} - \frac{\lambda}{4}) < a < \frac{\mu}{2}. \tag{8}$$

It is proved in [7] that such an energy density is polyconvex in the sense of Ball [3] when the constraints (8) are satisfied, which ensures the existence of solutions. Moreover this energy density becomes infinite when $\det(C) \to 0$, which is a desirable property: it ensures that no admissible deformation satisfies $\det(C) = 0$. We also use in Section 4 the description in terms of Young's modulus E and Poisson coefficient ν, the coefficient a still satisfiying (8).

The derivatives of the energy function with respect to the invariants are:

$$\begin{aligned}
\partial_1 \mathcal{W} &= a, \\
\partial_2 \mathcal{W} &= \frac{\mu}{2} - a, \\
\partial_3 \mathcal{W} &= \frac{\lambda}{4} - \frac{\mu}{2} + a - \left(\frac{\mu}{2} + \frac{\lambda}{4}\right) \frac{1}{i_3}.
\end{aligned}$$

We can deduce from this law the precise compatility condition between the compressive and circumferential stored strains. Under the assumption of spherical symmetry, we have in spherical coordinates:

$$T = \begin{pmatrix} T_{11} & 0 & 0 \\ 0 & T_{22} & 0 \\ 0 & 0 & T_{33} \end{pmatrix}$$

with

$$T_{11} = 2(a + (\frac{\mu}{2} - a)(3 + \alpha + 2\beta))\frac{(1+\alpha)^{1/2}}{1+\beta} - (\mu - 2a)\frac{(1+\alpha)^{3/2}}{1+\beta} + (2a - \mu + \frac{\lambda}{2})(1+\alpha)^{1/2}(1+\beta) - (\mu + \frac{\lambda}{2})\frac{1}{(1+\alpha)^{1/2}(1+\beta)}, \quad (9)$$

$$T_{22} = T_{33} = 2(a + (\frac{\mu}{2} - a)(3 + \alpha + 2\beta))\frac{1}{(1+\alpha)^{1/2}} - (\mu - 2a)\frac{1+\beta}{(1+\alpha)^{1/2}} + (2a - \mu + \frac{\lambda}{2})(1+\alpha)^{1/2}(1+\beta) - (\mu + \frac{\lambda}{2})\frac{1}{(1+\alpha)^{1/2}(1+\beta)}. \quad (10)$$

Note that from the mechanical point of view it may seem more natural to understand a stored stress, while from the numerical point of view the computations require to know the stored strain.

In practice we adopt the following procedure to determine a distribution of stored strain that meets the compatibility condition.

Data: The function $T_{11}(r)$ for $r \in [0, 1]$.
Result: The stored strains $\alpha(r)$ and $\beta(r)$
1- calculate $T_{22}(r) = T_{11}(r) + \frac{r}{2}T'_{11}(r)$;
2- for each r on a discrete grid, compute $\alpha(r)$ and $\beta(r)$ by solving the system (9)-(10) for the unknowns α, β;
Algorithm 1: Computation of an admissible stored stress distribution when the radial stored stress distribution T_{11} is given.

3.2 Numerical approach

The parameters of the material are the following:

$$\mu, \lambda, a.$$

The stored stress distribution is described by the function $r \mapsto T_{11}(r)$. Algorithm 1 from Section 3.1 allows to estimate the circumferential stored stress T_{22}, and the stored strain distribution described by α and β.

When the sphere is cut along a half plane at a given depth, the resulting displacement is symmetric w.r.t. the cutting plane. Therefore the simulation uses a half sphere as a domain, together with homogeneous Neumann condition along the incision, and homogeneous Dirichlet condition along the part of the symmetry plane that was not cut. The boundary condition is illustrated in Figure 3.

Our numerical simulations proceed as follows:

Data: μ, λ, a, $r \mapsto T_{11}(r)$ and d the incision depth.
Result: the displacement $\mathbf{u}$ after the incision
1- Compute $\alpha(r)$ and $\beta(r)$ using Algorithm 1;
2- Compute the stored left Cauchy-Green strain tensor $F^o F^{oT}$ from the value of α, β using Eq.(5) ;
3- Virtual incision: use the stored strain tensor $F^o F^{oT}$ in a half-sphere. Solve for the displacement $\mathbf{u}$;
Algorithm 2: Numerical incision of a sphere with stored stress

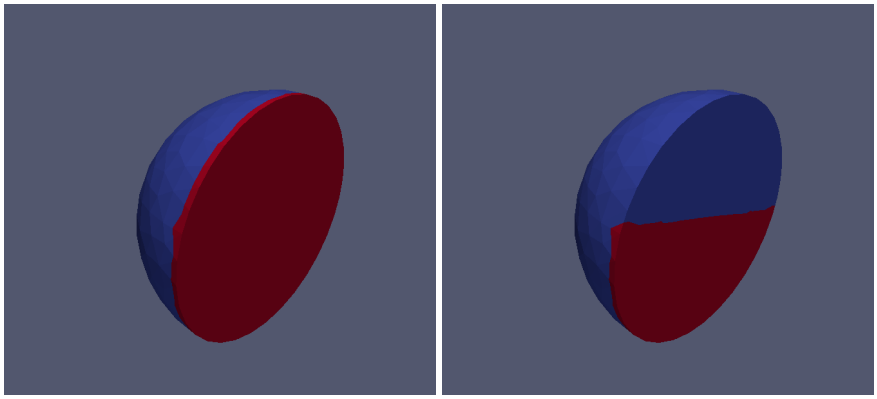

Fig. 3 Boundary condition to solve for the displacement, the sphere is cut along the xz-plane. In red : homogeneous Dirichlet condition along y direction, in blue: traction free surface (homogeneous Neumann). Left: the boundary condition for the initial domain, where the displacement field $\mathbf{u} \equiv 0$ is the solution. Right: the boundary condition for the incision, in this example the depth of the incision is half the diameter of the sphere.

The numerical simulations are implemented using Python and the finite elements library GetFem++ [20]. The mesh is generated using Gmsh [9].

The displacement field $\mathbf{u}$ is discretized using $P1$ finite elements. The non-linear elasticity problem is solved using a classical progressive loading method, where the stored strain is increased at each step, see *e.g.* [22]. At each increment of the load the following system is solved using a gradient descent:

$$\begin{cases} \text{div} T = 0 \ \Omega, \\ T.n = 0 \quad \partial\Omega, \end{cases} \tag{11}$$

where

$$\begin{aligned} T(\mathbf{u}) &= 2FS^o \\ &= \frac{2}{\det F^o}(\partial_1 \mathcal{W} + \partial_2 \mathcal{W} \text{Tr}(F^o F^{oT} F^T F)) F F^o F^{oT} - \frac{2}{\det F^o} \partial_2 \mathcal{W} F F^o F^{oT} F^T F F^o F^{oT} \\ &+ 2\partial_3 \mathcal{W} \det F^o \det(F)^2 F^{-T}. \end{aligned}$$

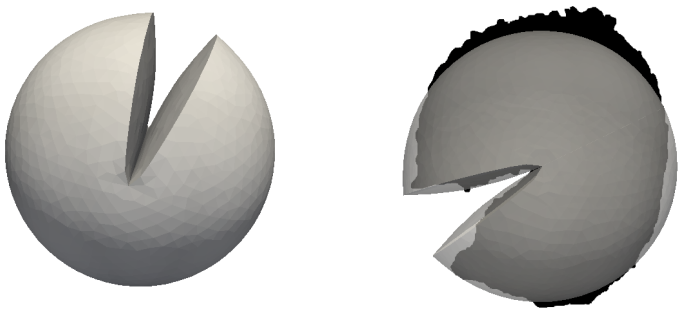

Fig. 4 Left: simulation of the displacement after an incision with depth 1 (half diameter of the sphere). The mechanical parameters are the following: $\nu = 0.46, E = 1, a = 0.6\mu/2$ and the radial stored stress is $T_{11}(r) = \gamma(r^2 - 1)$, where the constant γ is chosen so that the opening of the domain is equal to half of its radius. Right: superposition of the simulation and the binarized image of spheroid after the *in vitro* incision.

The weak formulation of (11) is

$$\forall \varphi \in H^1(\Omega, \mathbf{R}^3) \quad \int_\Omega T(\mathbf{u}) : \nabla \varphi = 0.$$

The update vector at each iteration of the gradient method is $\mathbf{h}$ that solves the linear tangent problem:

$$\forall \varphi \quad \int_\Omega T'(\mathbf{u}^k).\mathbf{h} : \nabla \varphi = -\int_\Omega T(\mathbf{u}^k) : \nabla \varphi.$$

We present in Figure 4 the deformed domain after the incision for one numerical simulation. This illustration is obtained using Paraview [12]. The simulation is performed on a half ball, and for a more natural rendering we present the complete domain obtained by adding the symmetric of the computed deformed domain. We present also the comparison with one experimental profile.

4 Parametric study

In this section we study numerically the influence of the parameters on the simulated displacement field. A parameter that has a small influence on the displacement field cannot be recovered from the *in vitro* experiments, since its value does not affect the measurements (or not significantly above the error level), even in the ideal case where the displacements of all points could be measured.

We proceed as follows: the domain is cut at a depth equal to 1 (the radius of the sphere). In order to obtain comparable displacement fields, for each value of the parameters the magnitude of the stored stress is normalized so

that the opening takes a prescribed value. The estimation of the influence of the parameters can be interpreted as the answer to the following question: 'for a given opening of the domain, what is the influence of the considered parameter on the precise shape of the deformed domain ?'.

4.1 Description of the parameters

Our mechanical model depends on several parameters: the material parameters and the parameters describing the stored stress. In this section, we list precisely these parameters and discuss on their ranges in our parametric study. All the parameters and values are summarized in Table 1.

First, the mechanical parameters that describe the Ciarlet-Geymonat material are: λ, μ and a. Second, the radial stored stress T_{11} is set to a power function for simplicity, described by the parameter n. The circumferential stored stress T_{22} is computed according to Equation (6). It yields

$$T_{11}(r) = \gamma \times (r^n - 1) \quad \text{and} \quad T_{22}(r) = \gamma \times \left[\left(1 + \frac{n}{2} \right) r^n - 1 \right]. \tag{12}$$

It is recalled that $T_{11}(r)$ must vanish at the boundary $r = 1$, because of the boundary condition (3). Also note that numerical tests show that when the function $r \mapsto T_{11}(r)$ is decreasing on the interval $[0, 1]$, and hence positive, the sphere tends to close after the numerical incision. This is not in accordance with the *in vitro* experiments that show an opening of the spheroid after incision. That is why the definition of this function is chosen such that it is increasing, which amounts to use positive values for γ. We present in Figure 5 the different profiles of stored stress, depending on the chosen value for the exponent n. Note that the radial component is always negative (compressive stress in the entire domain), while the circumferential component is negative inside the domain (tendency to "close" the domain tangentially) and positive in an outer layer (tendency to "open" the domain tangentially). The limit between these two zones and their relative magnitude depends on the exponent n. In other words, the exponent n describes the spatial distribution of stored stress in the domain: the higher is n, the more the circumferential stress is high close to the boundary of the domain, see Figure 5.

Let $\mathbf{u}_\infty$ be one-half of the maximum opening of the spheroid after the incision. The normalization of stored stress amounts to choose the coefficient γ in Equation (12). It is chosen such that the maximum opening $\mathbf{u}_\infty$ takes a prescribed value. We decided in our sensitivity analysis study to fix $\mathbf{u}_\infty = 0.5$, which amounts to say that the opening is equal to the initial radius of the spheroid (which is normalized to 1).

Since there is no hope to recover absolute value of the Lamé coefficients from the mere observation of displacements, we choose units in which the Young's modulus is $E = 1$. The Lamé parameters can then be described by Poisson coefficient ν using the expressions

$$\lambda = \frac{E\nu}{(1+\nu)(1-2\nu)}, \qquad \mu = \frac{E}{2(1+\nu)}.$$

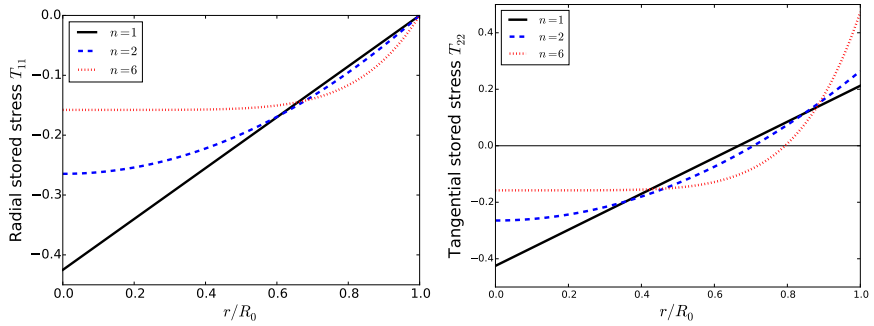

Fig. 5 Profile of the radial (left) and circumferential (right) stored stress for different values of the exponent n. For each value of n we plot $T_{11}(r) = \gamma(n) \times (r^n - 1)$ (left figure) and $T_{22}(r) = \gamma \times \left[\left(1 + \frac{n}{2}\right) r^n - 1\right]$ (right figure), where $\gamma(n)$ is chosen so that the opening is equal to the radius of the sphere. The different values of $\gamma(n)$ are given in Table 3

The limit value $\nu = 0.5$ corresponds to an incompressible material. Since biological tissues are almost incompressible, this study is performed for the range of $\nu \in (0.4, 0.5)$.

The parameter a belongs to $(a_{\min}, a_{\max})$, with $a_{\min} = \max(0, \frac{\mu}{2} - \frac{\lambda}{4})$ and $a_{\max} = \frac{\mu}{2}$, see eq. (8). It spans this entire interval and $a - a_{\min}$ is expressed as a fraction of $a_{\max} - a_{\min}$, as shown in Table 1.

The last parameter that is involved in the model is the exponent n that describes the spatial distribution of stored stress. Three values of n are tested in order to model linear stored stress ($n = 1$), parabolic stored stress ($n = 2$) and extreme stored stress ($n = 6$). The last case corresponds to a situation where at the boundary of the sphere the circumferential stored stress has a large magnitude. This represents an approximation to the intuition that 'compressive stress is inside the domain and circumferential stress is at the boundary'. Note that by increasing the exponent n one can achieve more extreme cases.

Table 1 The different values used for the three parameters of the model.

Parameter	Range	Discrete values tested in this study
ν	$(0, 0.5)$	0.4, 0.42, 0.44, 0.46, 0.48
$a' = \frac{a - a_{\min}}{a_{\max} - a_{\min}}$	$(0, 1)$	0.2, 0.4, 0.6, 0.8
n	$\mathbb{N}$	1, 2, 6

4.2 Quantitative study of the influence of the parameters

The prescribed maximum displacement $\mathbf{u}_\infty$ is similar for every simulation. Hence the maximum variation between two displacement fields can be expressed as a fraction of this maximum displacement. In order to study the effect of one parameter on the shape of the spheroid, two values (1) and (2) are first considered in the range spanned by the parameter of interest. Then for every couple of the other two parameters the maximum variations between the solutions $\mathbf{u}^{(1)}$ and $\mathbf{u}^{(2)}$ are computed, as well as the mean of all these variations. From a mathematical point of view, this reads

$$\|\Delta_B \mathbf{u}(n_1, n_2)\|_X = \frac{1}{|A \times C|} \sum_{(a',\nu)\in A\times C} \|\mathbf{u}(n_1, a', \nu) - \mathbf{u}(n_2, a', \nu)\|_X, \quad (13)$$

$$\|\Delta_A \mathbf{u}(a'_1, a'_2)\|_X = \frac{1}{|B \times C|} \sum_{(n,\nu)\in B\times C} \|\mathbf{u}(n, a'_1, \nu) - \mathbf{u}(n, a'_2, \nu)\|_X, \quad (14)$$

$$\|\Delta_C \mathbf{u}(\nu_1, \nu_2)\|_X = \frac{1}{|B \times A|} \sum_{(n,a')\in B\times A} \|\mathbf{u}(n, a', \nu_1) - \mathbf{u}(n, a', \nu_1)\|_X, \quad (15)$$

where B, A and C are the sets that contains the discrete values of n, a' and ν with $a' = (a - a_{\min})/(a_{\max} - a_{\min})$. The norm $\|\cdot\|_X$ is either the infinite norm, defined by $\|\mathbf{u}\|_\infty = \max_{\mathbf{x}\in\Omega} \|\mathbf{u}(\mathbf{x})\|$, or the average L^2 norm, defined by $\|\mathbf{u}\|_2 = \sqrt{\int_{\mathbf{x}\in\Omega} \|\mathbf{u}(\mathbf{x})\|^2 / Vol(\Omega)}$, where $Vol(\Omega)$ denotes the volume of the domain Ω.

The results are presented in Table 2, and we discuss below the results obtained with the infinite norm. The same comments hold qualitatively for the L^2 norm results, although their magnitude is about half the one with the infinite norm.

4.3 Discussion

The first comment concerns the value of a'. Table 1(b) shows that a variation of a' does not significantly change the displacement field. Not surprisingly, the largest difference comes by comparing the simulations performed with a' equals to 0.2 and 0.8, but it is less than 1% of the final opening of the spheroid. It can be asserted that the value of a' does not affect significantly the displacement field.

Similarly, the choice of Poisson coefficient ν in the range $[0.4, 0.5)$ close to incompressibility does not affect significantly the displacement field, since the extreme difference is of the order of 2%.

The last point is that the exponent n seems to be the most relevant parameter that impacts on the displacement field. It follows from the observation of Table 1(a) that the relative variation can be up to almost 5% between the extreme values. In order to provide a broader picture of the influence of the

(a) Percent $\|\Delta_B \mathbf{u}(n_1, n_2)\|_X / \mathbf{u}_\infty$, for all $(n_1, n_2) \in B$

n	1	2	6
6	1.54	4.91	
2	3.46		1.94
1		1.37	0.58

(b) Percent $\|\Delta_A \mathbf{u}(a_1, a_2)\|_X / \mathbf{u}_\infty$, for all $(a_1, a_2) \in A$

a'	0.2	0.4	0.6	0.8
0.8	0.60	0.42	0.22	
0.6	0.38	0.20		0.11
0.4	0.18		0.10	0.20
0.2		0.09	0.18	0.29

(c) Percent $\|\Delta_C \mathbf{u}(\nu_1, \nu_2)\|_X / \mathbf{u}_\infty$, for all $(\nu_1, \nu_2) \in C$

ν	0.4	0.42	0.44	0.46	0.48
0.48	2.14	1.79	1.38	0.85	
0.46	1.31	0.95	0.54		0.23
0.44	0.77	0.42		0.16	0.39
0.42	0.36		0.14	0.30	0.52
0.4		0.13	0.27	0.43	0.65

Table 2 Mean variations between the displacement fields given two values of one parameter, with respect to the two other parameters. The upper values correspond to the infinite norm and lower triangle to the L^2 norm.

exponent n on the displacement field, a series of simulations was performed enforcing a complete incision of the spheroid instead of the previous half cut (incision depth equal to 2). The increasing 'bending' of spheroid outline, that comes with large values of n, is highlighted on figure 6 (right).

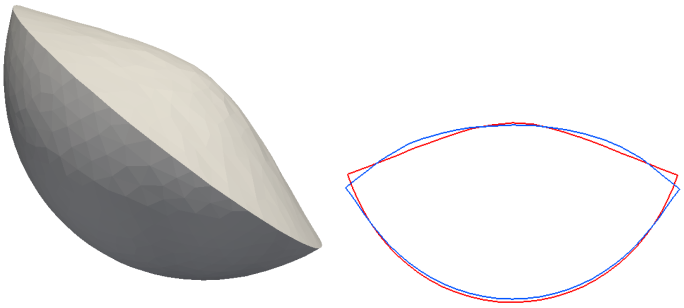

Fig. 6 Left: deformed domain after a complete incision ($n = 1$, $a' = .6$ and $\nu = .46$). Right: profiles of the domain along the plane $y = 0$ for two different values of n: Red: $n = 1$, $a' = .6$ and $\nu = .46$. Blue: $n = 6$, $a' = .6$ and $\nu = .46$. This documents the influence of n on the displacement field in the case of a complete incision.

As a conclusion of the parametric study: the parameters a' and ν do not affect significantly the displacement field (as long as ν is close to incompressibility), hence these parameters are not identifiable. Note that the parameter a' is specific to our hyperelastic model (Ciarlet-Geymonat) while ν is a classi-

cal elastic parameter. Since the Young's modulus is equal to 1 the knowledge of ν is equivalent of the knowledge of the Lamé parameters.

5 Coupling with experimental data

5.1 Experimental setup and measured quantities

Spheroids made from 500 HCT116 colon carcinoma cells and grown for 6 days were cut along diameter with an ophtalmic scalpel. Transmitted light images of spheroids were acquired before and 10s after incision under a Macrofluo Z16 APO microscope (Leica) fitted with a CoolSNAP ES2 CCD camera (Roper). The depth of the incision and the opening length (distance between the both extremities incised, see Figure 1) were measured using ImageJ software [21]. The measures of depth of incision and length of opening are reported as a percentage of the spheroid diameter. In Figure 7 are shown representative images of spheroids after cutting. The replicability of the experiment can be visualized however the variability does not allow to infer the precise shape of the boundary of the spheroid.

Note: The precise shape of the spheroid after incision would allow to estimate the parameter n. It is however difficult to estimate which value of n is the most close to experimental data because the difference between two simulations with different values of n is of the same order of magnitude as the variation between two replicas of the same *in vitro* experiment, and the bending profile in the experiment is difficult to quantify precisely, see Figure 7. We can conclude that the estimation of the precise shape of the boundary is out of reach of the present experiment, and the quantitative measurements that will be used are: the incision depth and the opening length.

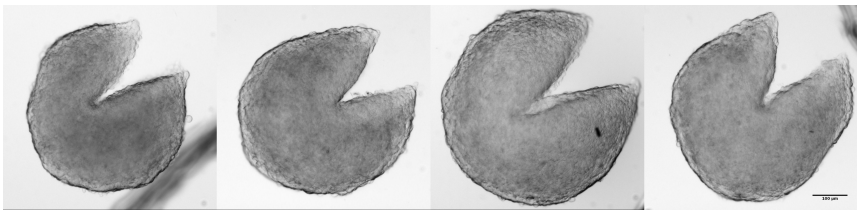

Fig. 7 Transmitted light images of four independent spheroids 10s after cutting. Scale bar: 100 microns.

5.2 Quantities that can be identified

In order to perform simulations to be compared to experimental data, we use the arbitrary values $a' = 0.6$ and $\nu = 0.46$. These values are arbitrary

and do not pretend to have any physical meaning. They are just required for computational purposes.

As also outlined above, in the experimental setup considered here the opening of the spheroid is approximately equal to its radius when it is cut in half. Therefore, assuming that the internal stress follows the law (12) with a given power n, there exists a unique coefficient γ that enforces a prescribed opening of $\omega = 0.5$. For each of the three exponents tested earlier, the numerical value of γ that constrains the opening $\omega = 0.5$ is given in Table 3. However the interpretation of γ is physically difficult to grasp and we consider the following quantities:

1) Total radial stored stress:

$$\sigma_{\text{rad}} = \int_{\Omega} T_{11} dx = 4\pi \int_{r} r^2 T_{11}(r)\, dr.$$

2) Total circumferential stored stress:

$$\sigma_{\text{tan}} = \int_{\Omega} (T_{22} + T_{33}) dx = 8\pi \int_{r} r^2 T_{22}(r)\, dr.$$

These quantities can be interpreted as total stored stresses necessary to deform the medium from the virtual unstressed configuration into the actual configuration before the incision. In other words they represent the amount of stress stored radially/circumferentially.

The unit to measure these stored stresses is a pressure unit $\times$ a volume unit, which provides an energy unit. The pressure unit is given by the Young's modulus, which we have normalized to 1, and the volume unit is the volume of the unit ball, since the domain Ω is the unit ball. Note that these quantities are computed analytically from Equations (12).

It is straightforward to prove, using Equation (6), that $\sigma_{\text{rad}} + \sigma_{\text{tan}} = 0$. In other words, the same amount of energy is stored as radial stress and as circumferential stress, only the sign is inverted.

The total radial stored stress was numerically estimated for different values of n. It follows from the observation of Table 3 that the quantity σ_{rad} has a small variation (approximately 1%) when the exponent n spans the range. In other words, we can assess that even if n is unknown, the value of σ_{rad} can be confidently recovered, or equivalently the value of σ_{tan} can be confidently recovered.

Table 3 Stored stress comparison between several power laws.

	$n = 1$	$n = 2$	$n = 6$
γ	0.425	0.265	0.158
σ_{rad}	-0.445	-0.445	-0.440

5.3 Comparison between experiments and simulation

The coefficient γ representing the magnitude of the stored stress is computed as before, such that the opening is 2ω when the incision depth is 1. The value of the half-opening ω was chosen so that the corresponding point belongs to the regression line of the experimental points. We found the value $\omega = 0.474$. Once the coefficient γ has been evaluated, the simulation is performed at different incision depths. For each depth the opening is computed and can be compared to experimental data. The results are presented in Figure 8 and show satisfactory agreement with experimental data.

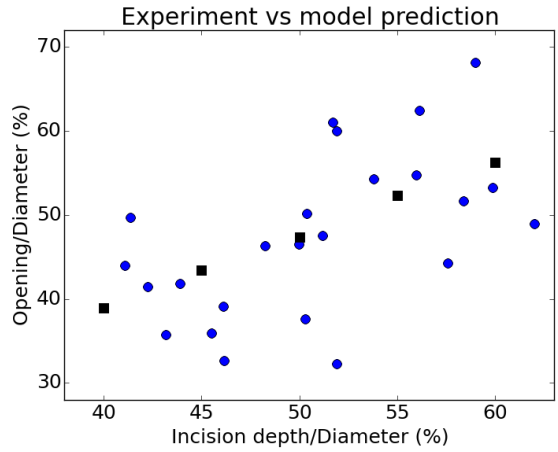

Fig. 8 Comparison between the experimental and the numerical relation between the opening length and incision depth.

6 Conclusion

We have studied in the present work the estimation of stored mechanical stress in spherical domains, with an application to spherical microtissues. The existence of stored mechanical stress is evidenced by the incision of the tissue which induces a change of shape, and the objective was to use incision experiments to obtain quantitative information regarding the stored stress. We have proposed contributions in the theoretical analysis, numerical parametric study and in the coupling with experimental data.

On the theoretical part, the spatial distribution of stored stress in a domain initially at rest cannot be arbitrary. We specify this constraint in the spherical case: the stored stress is the sum of a radial (compressive) component and a circumferential component which are not independent.

The parametric study shows the influence of the different parameters on the final shape of the domain after incision. If the shape of the domain after the incision is precisely measured, or in the case of complete incision, then one could recover the spatial distribution of the stored stress. In our model it is described by the exponent n. However the precise shape of the domain cannot be confidently estimated because of the uncertainty of the measurement due to the small scale of microtissues and the variability among the different samples.

In the realistic case where the available data is the opening distance vs incision depth, then the total radial stored stress can be evaluated, which is the amount of energy stored as stress that tends to 'inflate' the domain, or equivalently the total circumferential stored stress. In the absence of more information, no other parameters of the mechanical model can be confidently recovered. This conclusion follows the rule of a thumb that by measuring one real parameter, one cannot hope to recover more than one independent parameter.

References

1. Ambrosi, D., Ciarletta, P.: Plasticity in passive cell mechanics. International Journal of Non-Linear Mechanics **56**, 56–60 (2013)
2. Ambrosi, D., Preziosi, L.: On the closure of mass balance models for tumor growth. Mathematical Models and Methods in Applied Sciences **12**(05), 737–754 (2002)
3. Ball, J.M.: Convexity conditions and existence theorems in nonlinear elasticity. Archive for rational mechanics and Analysis **63**(4), 337–403 (1976)
4. Butcher, D.T., Alliston, T., Weaver, V.M.: A tense situation: forcing tumour progression. Nature Reviews Cancer **9**(2), 108–122 (2009)
5. Chuong, C.J., Fung, Y.C.: On residual stresses in arteries. Journal of Biomechanical Engineering **108**(2), 189–192 (1986)
6. Ciarlet, P.G.: Three-dimensional elasticity, vol. 20. Elsevier (1988)
7. Ciarlet, P.G., Geymonat, G.: Sur les lois de comportement en élasticité non linéaire compressible. CR Acad. Sci. Paris Sér. II **295**, 423–426 (1982)
8. Fennema, E., Rivron, N., Rouwkema, J., van Blitterswijk, C., de Boer, J.: Spheroid culture as a tool for creating 3d complex tissues. Trends in biotechnology **31**(2), 108–115 (2013)
9. Geuzaine, C., Remacle, J.F.: Gmsh: A 3-d finite element mesh generator with built-in pre-and post-processing facilities. International Journal for Numerical Methods in Engineering **79**(11), 1309–1331 (2009)
10. Grillo, A., Federico, S., Wittum, G.: Growth, mass transfer, and remodeling in fiber-reinforced, multi-constituent materials. International Journal of Non-Linear Mechanics **47**(2), 388–401 (2012)
11. Han, H., Fung, Y.: Residual strains in porcine and canine trachea. Journal of biomechanics **24**(5), 307,311–309,315 (1991)
12. Henderson, A., Ahrens, J., Law, C., et al.: The ParaView Guide. Kitware Clifton Park, NY (2004)
13. Johnson, B.E., Hoger, A.: The use of a virtual configuration in formulating constitutive equations for residually stressed elastic materials. Journal of Elasticity **41**(3), 177–215 (1995)
14. Jones, G.W., Chapman, S.J.: Modeling growth in biological materials. Siam review **54**(1), 52–118 (2012)
15. Liu, S., Fung, Y.C.: Zero-stress states of arteries. Journal of Biomechanical Engineering **110**(1), 82–84 (1988)
16. Mammoto, T., Mammoto, A., Ingber, D.E.: Mechanobiology and developmental control. Annual review of cell and developmental biology **29**, 27–61 (2013)

17. Marsden, J.E., Hughes, T.J.: Mathematical foundations of elasticity. Courier Corporation (1994)
18. Maugin, G.A.: Geometry and thermomechanics of structural rearrangements: Ekkehart kröner's legacy plenary lecture presented at the 80th annual gamm conference, augsburg, 25-28 march 2002. ZAMM-Journal of Applied Mathematics and Mechanics/Zeitschrift für Angewandte Mathematik und Mechanik **83**(2), 75–84 (2003)
19. Omens, J.H., Fung, Y.C.: Residual strain in rat left ventricle. Circulation Research **66**(1), 37–45 (1990)
20. Renard, Y., Pommier, J.: Getfem+ (2006)
21. Schneider, C.A., Rasband, W.S., Eliceiri, K.W.: Nih image to imagej: 25 years of image analysis. Nature methods **9**(7), 671 (2012)
22. Simo, J.C., Hughes, T.J.: Computational inelasticity, vol. 7. Springer Science & Business Media (2006)
23. Stylianopoulos, T., Martin, J.D., Chauhan, V.P., Jain, S.R., Diop-Frimpong, B., Bardeesy, N., Smith, B.L., Ferrone, C.R., Hornicek, F.J., Boucher, Y., et al.: Causes, consequences, and remedies for growth-induced solid stress in murine and human tumors. Proceedings of the National Academy of Sciences **109**(38), 15,101–15,108 (2012)
24. Xie, J., Liu, S., Yang, R., Fung, Y.C.: The zero-stress state of rat veins and vena cava. Journal of Biomechanical Engineering **110**(1), 82–84 (1988)